INSTITUTE OF PHYSICS PUBLISHING JOURNAL OF PHYSICS D: APPLIED PHYSICS
J. Phys. D: Appl. Phys. **38** (2005) 1644–1648 doi:10.1088/0022-3727/38/11/002

# Recent advances in microcavity plasma devices and arrays: a versatile photonic platform

**J G Eden, S-J Park, N P Ostrom and K-F Chen**

Laboratory for Optical Physics and Engineering, Department of Electrical and Computer Engineering, University of Illinois, Urbana, IL 61801, USA

Received 1 December 2004, in final form 1 February 2005
Published 20 May 2005
Online at stacks.iop.org/JPhysD/38/1644

**Abstract**
Selected highlights in the recent development of microplasma devices are reviewed with emphasis on large arrays of Si-based hybrid plasma/semiconductor pixels. Arrays of 40 000 (200 × 200) pixels, excited by sinusoidal ac waveforms at frequencies of 5–20 kHz, have now been realized. The fabrication of these arrays and their electrical and optical performance with rare gases and $Ar/N_2$ mixtures are briefly described. Metal/dielectric/metal devices having a piezoelectric dielectric ($BaTiO_3$), a cylindrical microcavity 50 $\mu$m in diameter, and a total thickness of ∼110 $\mu$m are also discussed. Finally, the introduction of multiwall carbon nanotubes into microdischarge devices as an auxiliary source of current is presented as being exemplary of the opportunities afforded by the integration of nanotechnology into microcavity plasma structures.

## 1. Introduction

Lying at the intersection of plasma science, photonics and materials science, microplasma device science and technology offers not only a new realm of plasma phenomenology but also device functionality [1, 2]. Confining weakly ionized plasmas to microcavities having characteristic dimensions below 100 $\mu$m, and bounded by semiconductor, electro- or magneto-optical, piezoelectric, or nanostructured materials, presents a broad array of *photonic* device options, in particular. The opportunity to interface a gas phase plasma with the electron–hole plasma generated in conventional semiconductor devices is especially intriguing and only recently have exploratory efforts begun and prototype devices reported [3, 4].

Recent examples of microplasma devices developed in our laboratory primarily for photonics applications are briefly reviewed here. A milestone in the development of large arrays of microplasma devices has been reached. Arrays as large as 40 000 pixels, each of which is an inverted pyramid device, have been fabricated and operated in rare gases under ac excitation (typically 5–20 kHz). Exhibiting extraordinary pixel-to-pixel emission uniformity, these arrays are well-behaved electrically and optically and appear to be of value as microdisplays and in biomedical diagnostics. Metal/dielectric/metal structure devices incorporating the piezoelectric material barium titanate ($BaTiO_3$) will also be discussed. Finally, an example of the potential of nanotechnology to impact microplasma device operation is presented. The growth of carbon nanotubes (CNTs) directly into the cavity of microplasma devices influences positively all of the key parameters of the device, including operating voltage and radiative efficiency.

## 2. Large arrays of ac-excited silicon pixels

In 1997, the first microplasma devices fabricated in Si were reported [5] and inverted square pyramid structures were introduced in 2001 [6]. To date, devices with pyramidal microcavities having emitting apertures (i.e. base dimensions) as small as 10 × 10 $\mu m^2$ have been demonstrated [2] but larger structures will be emphasized here. Early devices employed a dry etchable polyimide as the sole dielectric and the dc-driven arrays were limited in size to 5 × 5 pixels. Subsequent alterations in the device structure and the dielectric, in particular, led to the successful demonstration of arrays as large as 15 × 15 but unacceptable emission nonuniformities remained [7, 8].

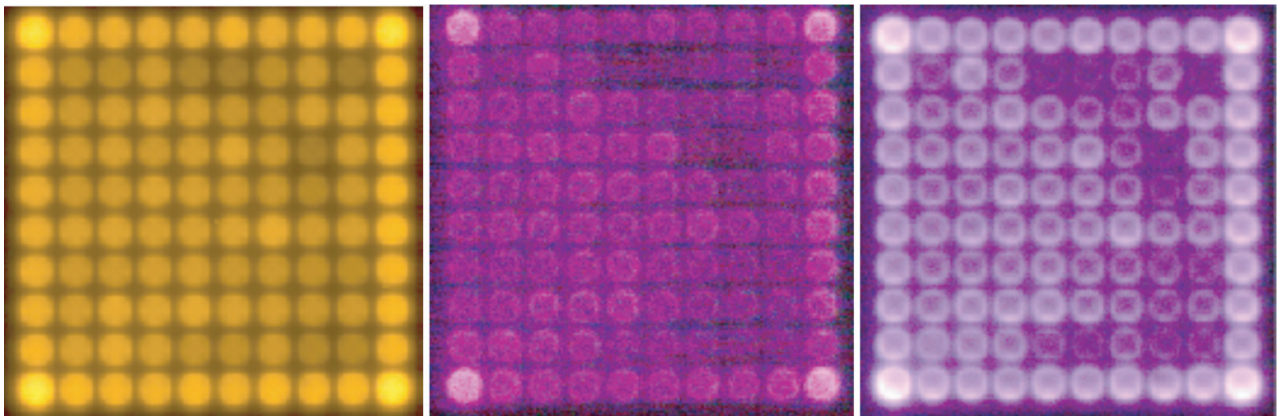

**Figure 1.** Photographs (top view) of a $10 \times 10$ array of $(50\,\mu\text{m})^2$ inverted square pyramid devices operating dc in (left to right): 800 Torr Ne, 400 Torr Ar and 400 Torr of an Ar/5% $N_2$ mixture. Owing to an artefact of the CCD camera, the Ne emission is not as yellow as the left image suggests.

### *2.1. Emission nonuniformities in dc-excited arrays*

Over the past several years, considerable effort invested in developing the fabrication processes for these microcavity pixels has resulted in clear improvements in the uniformity of the pixels themselves as well as the emission generated. As an example, figure 1 presents three photographs (obtained with a CCD camera and a telescope) of a recently fabricated $10 \times 10$ array of $(50\,\mu\text{m})^2$ inverted pyramid Si devices. Representative of those observed for the other arrays produced to date, these images show that the emission uniformity is acceptable for the lighter rare gases such as Ne (figure 1, left image), although the pixels at the perimeter of the array are brighter than those in the interior. Weak visible emission is produced by Ar (central image of figure 1) since its strongest atomic transitions generate radiation in the near-infrared and ultraviolet but, upon close inspection, trends similar to those in Ne are observed. Distinct emission nonuniformities are apparent when the array is operated in an Ar/5% $N_2$ gas mixture at a total pressure of 400 Torr (figure 1, right image). Note that the inner pixels are again fainter than those at the perimeter. Also, the enhancement of emission around the edge of each pixel, owing to the comparative strength of the electric field, is evident. It appears that the spatial variation of the fluorescence intensity is a visual representation of current flow in the thin ($0.2\,\mu$m thick) Ni anode that provides power to all the pixels. In this device design, the array has a single anode contact that lies to the left of the array in each photograph of figure 1. Consequently, the brightest pixels are those on the left, nearest to the power feed. Current density in this, essentially two-dimensional, anode has both longitudinal and transverse components, which are responsible for the pixel emission intensity distribution. We are confident that further development of the array design, and detailed analysis of anode layout and characteristics, specifically, will ameliorate the difficulties described above and improve the uniformity of power distribution to all pixels in large, dc-excited microplasma arrays.

### *2.2. AC-driven,* $200 \times 200$ *pixel arrays*

In a different approach to addressing the limitations described above, we have recently designed, fabricated, and successfully tested arrays of $50 \times 50\,\mu\text{m}^2$ Si devices that are as large as $200 \times 200$ ($4 \times 10^4$) pixels and excited by a sinusoidal ac or bipolar waveform. Although the microcavity continues to have the form of an inverted square pyramid, the pixel structure (cf figure 2) differs significantly from that of the dc device. Once the microcavity is produced by wet etching, a $2\,\mu$m thick film of silicon nitride is grown over the interior surface of the microcavity and around its aperture (i.e. base of the pyramid) by low pressure chemical vapour deposition. A second dielectric film (polyimide and/or $SiO_2$) is subsequently deposited only outside the microcavity, followed by a thin ($0.2\,\mu$m) Ni film that serves as a second electrode. Another $2\,\mu$m thick film of silicon nitride, covering the inside of the microcavity and the dielectric/metal electrode structure, completes the fabrication process. Devices having this design have proven to be robust electrically and chemically, and yield arrays with extraordinary pixel-to-pixel emission uniformity.

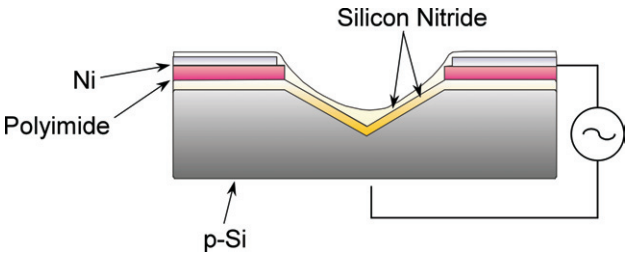


**Figure 2.** Cross-sectional diagram (not drawn to scale) of a Si inverted pyramid device designed for excitation by sinusoidal ac or bipolar voltage waveforms. The device dimensions are specified by the area of the square pyramidal microcavity at its aperture (i.e. base of the pyramid).

Figure 3 is an optical micrograph of a segment of a $50 \times 50$ pixel array operating in Ne at 700 Torr and excited by a sinusoidal ac voltage waveform with a frequency of 15 kHz. As noted above, the individual pixels comprising the array are $50 \times 50\,\mu\text{m}^2$ at the base of the microcavity and the device pitch (centre-to-centre separation) is $100\,\mu$m. Consequently, the device packing density is $10^4\,\text{cm}^{-2}$ and the active area of the array is $0.25\,\text{cm}^2$. Voltage–current ($V$–$I$) characteristics for the $50 \times 50$ arrays are presented in figure 4 for 500 Torr of

**Figure 3.** Segment of a 50 × 50 pixel array of 50 × 50 $\mu$m$^2$ Si devices operated in 700 Torr of Ne at 15 kHz. The RMS voltage and current are 250 V and 9.0 mA, respectively.

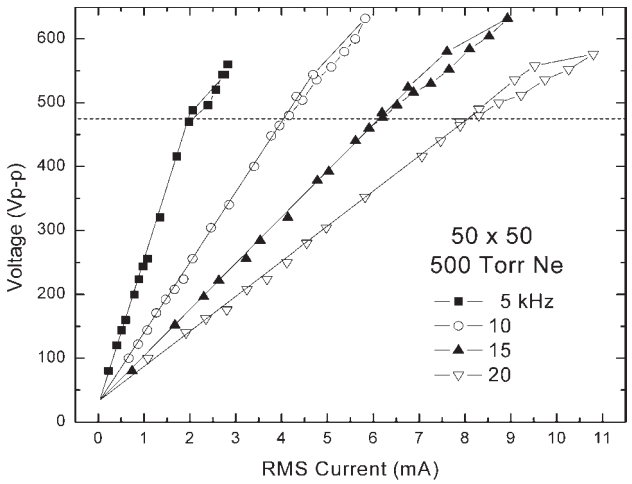


**Figure 4.** $V$–$I$ characteristics for a 2500 (50 × 50) array of (50 $\mu$m)$^2$ pixels in Si operating in 500 Torr of Ne. Note that all voltages are given in terms of their peak-to-peak values. Also, the dashed horizontal line denotes the voltage at which all pixels ignite, irrespective of whether the ac excitation frequency is 5, 10, 15 or 20 kHz.

Ne and sinusoidal ac excitation frequencies of 5, 10, 15 and 20 kHz. The reproducibility of these measurements is such that the uncertainty in the data (±1 V) is smaller than the size of the symbols in figure 4. Regardless of the driving frequency, all pixels ignite simultaneously at a peak-to-peak voltage of 470 ± 5 V. Below ignition voltage, the $V$–$I$ characteristics are dominated by the capacitive reactance of the array structure, and significant reductions in the reactive power consumption will undoubtedly be realized in the near future as more effort is devoted to optimizing the array design. As indicated by the data of figure 4, the presence of plasma in the pixels reduces the overall resistance of the load and a small degree of hysteresis is observed consistently in the $V$–$I$ characteristics.

Within the past year, we have fabricated and operated larger arrays, comprising 40 000 (50 $\mu$m)$^2$ pixels in a 200 × 200 array having an active area of 4 cm$^2$. Photographs of an array operating in Ne at 700 Torr are shown in figure 5 and one is immediately struck by the uniformity of the pixel-to-pixel emission. Lineouts of the relative emission from columns and rows of pixels, derived from digital images, indicate that the emission is uniform across the entire array to within ±10%. Once again, all pixels ignite simultaneously at a voltage dictated by the gas itself and its pressure. For $p_{Ne} = 900$ Torr, the threshold voltage is 194±2 V (RMS) at 10 kHz and a visual inspection of the pixels with a telescope shows the discharge within each microcavity to be a uniform glow.

Other gases and gas mixtures are currently under investigation in 50 × 50 arrays. Mixtures of 2% $N_2$ in Ar, for example, produce strong emission on the well-known C→B transition of $N_2$ in the near-ultraviolet. The $V$–$I$ characteristics of the array for total gas pressures in the 500–900 Torr range are virtually indistinguishable from one another. For a total mixture pressure of 500 Torr (∼490 Torr Ar, 10 Torr $N_2$), the 2500 pixel array draws ∼8 mA of RMS current for a voltage of 317 V (RMS) and an excitation frequency of 10 kHz. Further details regarding the performance of large Si arrays with these and other gaseous and vapour emitters will be reported elsewhere.

## 3. Multilayer structures with a piezoelectric dielectric

A recurring theme in microdischarge science and technology is the profound impact of the dielectric in shaping the electric field within the microcavity and, therefore, the electrical and optical characteristics of the device. Two years ago, we reported [9] the design and performance of dc-excited multilayer Ni/dielectric/Ni device structures in which the dielectric was a film of $Al_2O_3$ or BN. This design is being pursued for applications requiring robust chemical and thermal properties, but the flexibility of the finished structure (typically ∼105–170 $\mu$m in thickness) and the wide variety of dielectric films available by casting and sol-gel processing, for example, make this device structure an attractive test bed for examining microcavity discharge behaviour.

Additional data are reported here for devices in which the piezoelectric material barium titanate ($BaTiO_3$) serves as the dielectric and the cylindrical microcavity has a diameter of 50 $\mu$m. Four layer devices having a Ni/$BaTiO_3$/polyimide/Ni structure were constructed in which the Ni electrodes are fabricated from 50 $\mu$m thick foil. A stack of $BaTiO_3$ films, having a total thickness of 5 $\mu$m, was deposited onto one electrode by a sol–gel process and the thickness of the next film—polyimide—was also ∼5 $\mu$m, bringing the total thickness of the device to ∼110 $\mu$m. After construction, the device (or array of devices) was baked to cure the dielectric and desorb the organic binder. The $V$–$I$ data of figure 6, obtained with dc excitation, illustrate the behaviour of the device if the processing ends with a 'soft bake' at 180°C. Results are shown for Ne gas pressures between 400 and 900 Torr and it is clear that the devices operate in the abnormal glow mode over most of the available operating range. Operating voltages as low as ∼98 V are measured for $p_{Ne} = 900$ Torr. If, however, the device is baked at a much higher temperature (650°C) prior to being tested, the $V$–$I$ characteristics are altered significantly (cf figure 7). Operating voltages rise only 2–4 V at higher pressures (⩾800 Torr) but by more than 10 V at the lowest

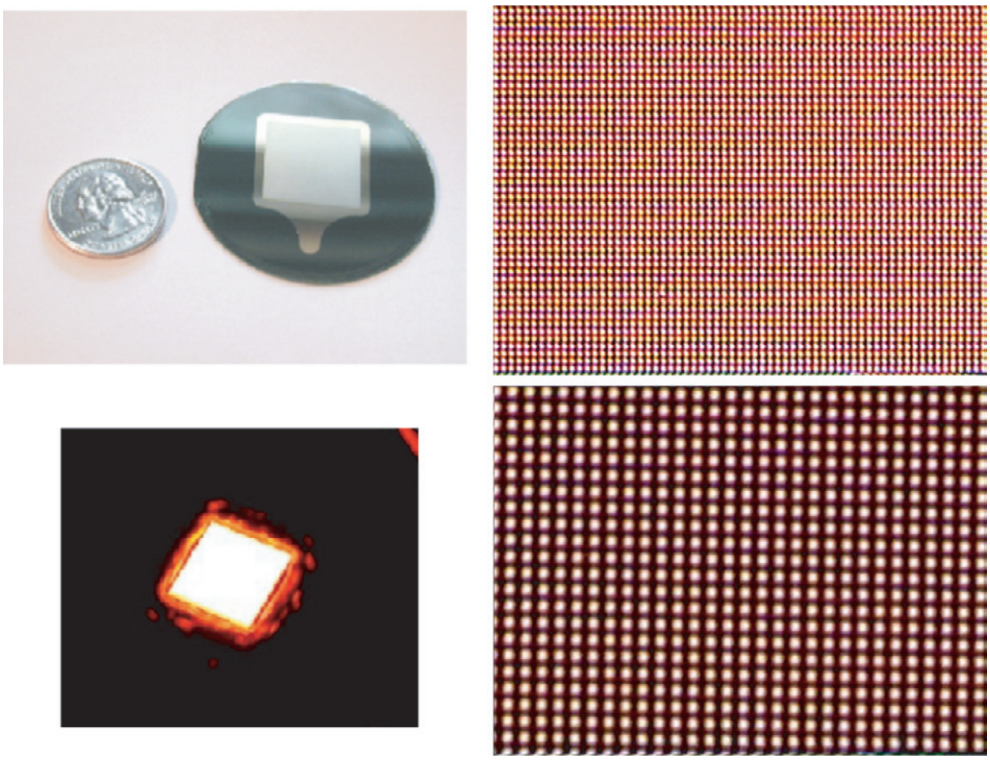

**Figure 5.** (Right) Optical micrographs (recorded with a telescope and CCD camera) of segments of a 200 × 200 array, shown for two degrees of magnification. On the left, photographs of the finished array and its appearance when operating at $p_{Ne} = 700$ Torr are shown.

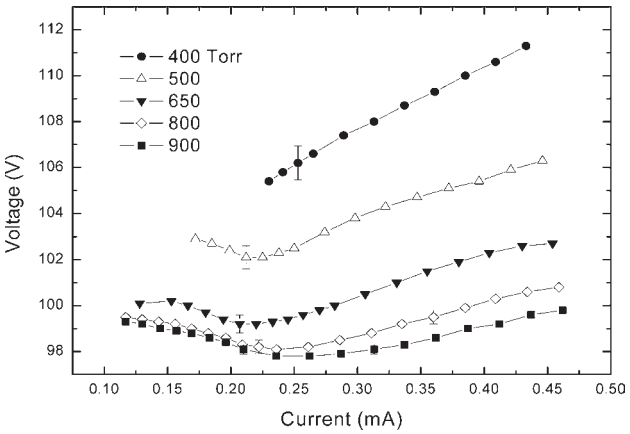


**Figure 6.** $V$–$I$ characteristics for the dc operation of a Ni/5 $\mu$m $BaTiO_3$/5 $\mu$m polyimide/Ni microplasma device with a cylindrical microcavity 50 $\mu$m in diameter. The device has been soft-baked at 180°C prior to operation. Data are shown for Ne pressures between 400 and 900 Torr.

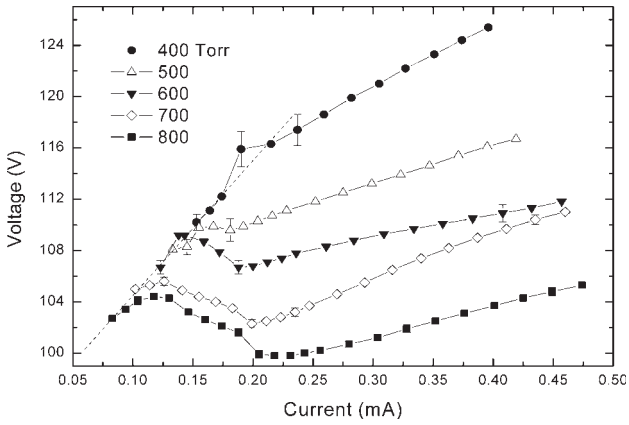


**Figure 7.** Data similar to those of figure 5 except that the $BaTiO_3$ dielectric-containing device was baked at 650°C. The dashed line has a slope of ∼107 kΩ.

pressures examined. More importantly, the characteristics themselves are changed noticeably. At all pressures studied, the devices function stably at currents below ∼150 $\mu$A, which was possible with the device of figure 6 only at higher pressures ($\geqslant$650 Torr). The result is that the characteristics of figure 7 approach a limit at low currents, converging on the line indicated, which has a slope of ∼107 kΩ. For $p_{Ne} \geqslant 600$ Torr, this behaviour yields a local maximum in the voltage, and a narrow region with a negative slope that resembles the Townsend mode. For $p_{Ne} < 500$ Torr, this intermediate region vanishes. At higher currents, the characteristics all display a similar slope (and, therefore, plasma resistance). It is clear, then, that the device characteristics may be altered by the device fabrication process and it must be emphasized that the characteristics of both figures 6 and 7 are stable indefinitely. Therefore, these data provide a vivid reminder of the fact that the performance of microdischarge devices is grounded in the specific properties of the dielectric (or dielectric stack) and the microcavity geometric cross section.

## 4. Incorporation of CNTs into a microplasma device

CNTs are well known for their field-emission properties which are a result of their extraordinary aspect ratios (∼$10^2$–$10^3$).

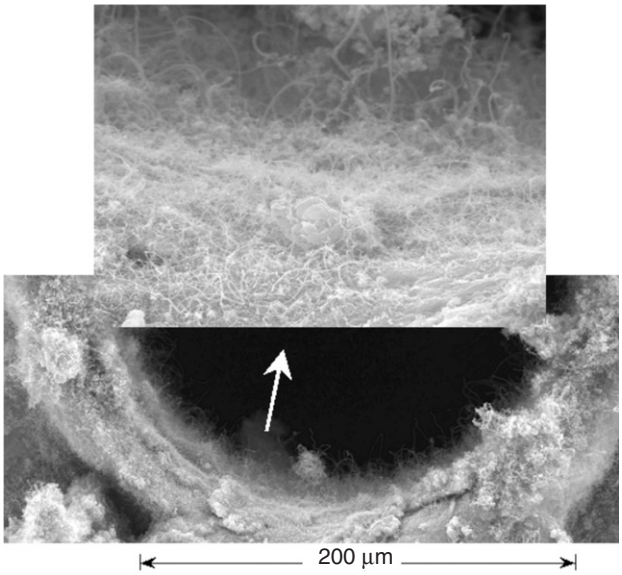


**Figure 8.** Electron micrographs of CNTs grown directly into the 200 $\mu$m diameter microcavity of a Ni/BN/Ni microplasma device. The lower portion of the figure shows the CNTs within the cathode (viewed end-on) and around its aperture, whereas the inset (upper portion of the figure) is a magnified view of the multiwall nanotubes.

In an effort to explore the potential of nanostructures in enhancing the performance of microplasma devices, multiwall CNTs were incorporated directly into the cylindrical cathode of Ni screen/BN/Ni devices similar to those discussed in the last section [10, 11]. Having cylindrical microcavities 200 $\mu$m in diameter and a boron nitride dielectric film $\sim$70 $\mu$m in thickness, the microplasma devices are durable, enabling CNTs to be grown within the microcavity by hot filament chemical vapour deposition at 700°C. Scanning electron micrographs such as those in figure 8, in which the microcavity is viewed along its axis, show the CNTs to be multiwall with nominal diameters of 40–80 nm. Experimentation with the vapour deposition process was necessary to ensure the growth of CNTs within the cathode *without* electrically shorting the device.

The turn-on electric field strength of nanotubes grown in this manner on Si was measured to be $\sim$2.5 V $\mu$m$^{-1}$ (for a current density of 2 nA cm$^{-2}$), a value readily provided by the axial *and* radial components of the electric field within the microcavity under normal operating conditions. That is, we take advantage of the fact that the electric field strength normally present within a Ni/dielectric/Ni structure device, in the vicinity of the cathode wall, is more than sufficient to activate the CNTs as field emitters. It is important to note that the CNTs in this application provide an auxiliary source of electrons and do so in the critical region of the discharge near the interior surface of the cathode.

The effect of introducing CNTs on the performance of the microcavity plasma devices is dramatic. Operating voltages in Ne drop by as much as 22%, ignition voltages fall by 14–18% in the 100–300 Torr pressure region, and radiative efficiency in the 300–800 nm wavelength interval *increases* by 6–9% over the entire pressure range studied (200–600 Torr of Ne) [10, 11]. In short, all of the key operational parameters of the microplasma device are improved significantly by the presence of the nanotubes. These results suggest that the full implementation of nanotechnology into the design and processing of microplasma devices and arrays will be necessary to realize their full potential.

## 5. Summary and conclusions

Bringing new materials, device designs and processing techniques to bear on microplasma device technology continues to yield dividends in terms of improved performance and lifetime, as well as expanded functionality. Arrays of $4 \times 10^4$ pixels are now available in 4 cm$^2$ of Si and we see no significant barriers to developing arrays of much larger active areas ($>$100 cm$^2$). Silicon has the enormous advantage of offering the ability to design and fabricate individual devices and arrays with precision, and the latter in virtually any pattern to achieve specific optical characteristics. We expect this asset will prove to be of considerable value in interfacing microplasma emitter arrays with other photonic devices and systems.

Adopting thick and thin film materials deposition processes offers the microplasma community tools with which to grade or 'fine tune' the electric field within the microcavity. Perhaps, most exciting is the emerging opportunity to fully integrate nanotechnology into microplasma device design. Exploiting the field emission properties of CNTs as described here and in [10, 11] is only one example of the potential of nanostructures to, for example, enhance or tailor the emission from a single device or an array.

## Acknowledgments

The technical assistance of K Collier and the support of this work by the US Air Force Office of Scientific Research under grant nos F49620-03-1-0391 and F49620-02-C-007 are gratefully acknowledged.

## References

[1] Eden J G *et al* 2003 *J. Phys. D: Appl. Phys.* **36** 2869
[2] Park S-J, Chen J, Wagner C J, Ostrom N P, Liu C and Eden J G 2002 *IEEE J. Sel. Topics Quantum Electron* **8** 387
[3] Park S-J, Eden J G and Ewing J J 2002 *Appl. Phys. Lett.* **81** 4529
[4] Wagner C J, Park S-J and Eden J G 2001 *Appl. Phys. Lett.* **78** 709
[5] Frame J W, Wheeler D J, DeTemple T A and Eden J G 1997 *Appl. Phys. Lett.* **71** 1165
[6] Park S-J, Chen J, Liu C and Eden J G 2001 *Appl. Phys. Lett.* **78** 419
[7] Park S-J, Eden J G, Chen J and Liu C 2001 *Appl. Phys. Lett.* **79** 2100
[8] Park S-J, Eden J G, Chen J, Liu C and Ewing J J 2001 *Opt. Lett.* **26** 1773
[9] Park S-J and Eden J G 2003 *Electron. Lett.* **39** 773
[10] Park S-J, Eden J G and Park K-H 2004 *Appl. Phys. Lett.* **84** 4481
[11] Park S-J, Park K-H and Eden J G 2004 *Electron. Lett.* **40** 563